

Acceleration of electromagnetic shower development and enhancement of light yield in oriented scintillating crystals

Mattia Soldani,^{1,*} Pietro Monti-Guarnieri,^{2,3} Alessia Selmi,^{4,5} Nicola Argiolas,^{6,7} Luca Bomben,^{4,5} Claudia Brizzolari,^{4,5} Nicola Canale,⁸ Stefano Carsi,^{4,5} Nikolaos Charitonidis,⁹ Davide De Salvador,^{6,7} Vincenzo Guidi,^{8,10} Viktor Haurylavets,¹¹ Mikhail Korzhik,¹¹ Giulia Lezzani,^{4,5} Alexander Lobko,¹¹ Lorenzo Malagutti,⁸ Sofia Mangiacavalli,^{4,5} Valerio Mascagna,¹² Andrea Mazzolari,^{8,10} Vitaly Mechinsky,¹¹ Matthew Moulson,¹ Riccardo Negrello,^{8,10} Gianfranco Paternò,⁸ Leonardo Perna,^{4,5} Christian Petroselli,^{4,5} Michela Prest,^{4,5} Marco Romagnoni,^{8,10} Federico Ronchetti,¹³ Giosué Saibene,^{4,5} Francesco Sgarbossa,^{6,7} Alexei Sytov,⁸ Viktor Tikhomirov,¹¹ Erik Vallazza,^{5,3} and Laura Bandiera^{8,†}

¹*INFN Laboratori Nazionali di Frascati, Frascati, Italy*

²*Università degli Studi di Trieste, Trieste, Italy*

³*INFN Sezione di Trieste, Trieste, Italy*

⁴*Università degli Studi dell'Insubria, Como, Italy*

⁵*INFN Sezione di Milano Bicocca, Milan, Italy*

⁶*Università degli Studi di Padova, Padova, Italy*

⁷*INFN Laboratori Nazionali di Legnaro, Legnaro, Italy*

⁸*INFN Sezione di Ferrara, Ferrara, Italy*

⁹*CERN, Meyrin, Switzerland*

¹⁰*Università degli Studi di Ferrara, Ferrara, Italy*

¹¹*Institute for Nuclear Problems, Belarusian State University, Minsk, Belarus*

¹²*Università degli Studi di Brescia, Brescia, Italy*

¹³*École Polytechnique Fédérale de Lausanne, Lausanne, Switzerland*

(Dated: April 19, 2024)

We observed a substantial increase of the scintillation light output of lead tungstate (PbWO₄) at a small incidence angle with respect to two main lattice axes. This reflects the acceleration of electromagnetic shower development that occurs in the crystalline Strong Field. We measured the scintillation light generated by 120-GeV electrons and 10-100-GeV γ rays on thick samples. This result deepens the knowledge of the shower development mechanisms in crystal scintillators and could pave the way to the development of innovative accelerator- and space-borne calorimeters.

Inorganic crystal scintillators are essential in high-energy, nuclear, medical and astroparticle physics, allowing precise measurements of the energy of electrons, positrons and γ rays. In particular, high-energy physics (HEP) and astroparticle physics experiments commonly rely on high-resolution electromagnetic calorimeters based on inorganic scintillating crystals, in which the energy of the incident particle is measured detecting the light resulting from the electromagnetic shower it initiates [1]. At the energy frontier (i.e., from the multi-GeV range up), showers can extend over ten or more radiation lengths (X_0), which requires high-atomic-number (Z), dense crystals with a small X_0 for compact detectors to fully contain them.

The formation of electromagnetic showers in inorganic scintillators is conventionally modeled as occurring in amorphous media. This approach accounts for bremsstrahlung radiation emission and electron-positron pair production, respectively by electrons/positrons and γ rays interacting with the Coulomb potential of single atoms. However, these models neglect the significant impact of the crystalline lattice and of its orientation: specifically, when a particle moves close to one of

the strings (axes) of atoms in the lattice, it experiences an electromagnetic field that is approximately constant along the string direction, resulting from the coherent sum of the single-atom contributions. This phenomenon fundamentally alters the electromagnetic processes [2, 3].

At sufficiently high energy, the lattice field in the particle rest frame is Lorentz-boosted [2–5] and can reach an amplitude larger than the Schwinger critical field ($\mathcal{E}_0 = m_e^2 c^3 / e \hbar \sim 1.32 \cdot 10^{16}$ V/cm), i.e. the threshold for nonlinear QED effects [6]. This is the so-called Strong Field (SF) regime [3]. Such an intense field induces an enhancement of the radiation emission probability with respect to the Bethe-Heitler description typical of amorphous media [7]. By crossing symmetry, the probability for the creation of an e^\pm pair by a high-energy photon is significantly increased as well [2, 3, 8, 9].

The SF regime is attained if $\chi = \gamma \mathcal{E}_{\text{lab}} / \mathcal{E}_0 \gtrsim 1$, where \mathcal{E}_{lab} is the axial electric field in the laboratory frame and γ is the Lorentz factor, which translates into an energy threshold for the primary particle [2–4]. This energy scale is of $\gtrsim 10$ GeV for high- Z materials and is roughly the same for both bremsstrahlung and pair production: for the latter, it can be estimated by replacing γ with $\gamma_{\text{PP}} = \hbar\omega / m_e c^2$, $\hbar\omega$ being the incident photon energy. The SF effect intensity grows with χ up to saturation, which is typically reached above several TeV, far beyond current experimental conditions [3].

* mattia.soldani@lnf.infn.it

† bandiera@fe.infn.it

Overall, the SF-related increase of these processes leads to an acceleration of the electromagnetic shower development with respect to the case of an amorphous or randomly oriented medium. In case of a scintillating crystal, the larger number of secondary particles leads to an increase of the number of scintillation photons emitted inside the medium within the same distance.

For instance, let us consider lead tungstate (PbWO_4 , $X_0 \sim 0.89$ cm [10]), one of the most commonly used inorganic scintillators, and two of its main axes, $\langle 100 \rangle$ and $\langle 001 \rangle$ – shown in figure 1 top. In case of the considered axes, the full SF regime ($\chi = 1$) is attained at an energy of about 25 GeV. The corresponding values of U_0 , i.e. the depth of the potential well associated to the axial field [3], are approximately 460 eV and 420 eV respectively [11]. An estimate of the misalignment angle (θ_{mis}), i.e., the relative angle between the incidence direction and the crystallographic axis, needed for the SF shower development acceleration to be achieved is provided by $\Theta_0 = U_0/m_e c^2$ [3], thus the angular acceptance of the SF regime is about 0.9 mrad in both cases.

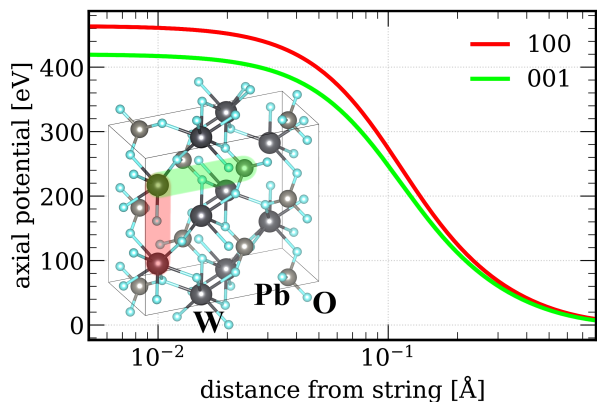


FIG. 1. Top: single-atomic-string potentials of two of the main PbWO_4 axes as a function of the distance from the atomic string. The corresponding crystalline structure is shown in the insertion. Bottom: experimental setup for the measurements with electron beams on the CERN H2 beam-line.

For $\theta_{\text{mis}} > \Theta_0$, other coherent effects occur, i.e., coherent bremsstrahlung and coherent pair production [12, 13]. It has been observed that such phenomena determine an increase of both bremsstrahlung and pair production for θ_{mis} up to 1° and also for energies significantly smaller than the SF scale [14].

Experimental investigations of the SF effects in both radiation emission [15] and pair production [16] started in the 1980s. They were initially focused on very thin

($\lesssim 1$ mm) silicon, germanium and diamond crystals. Studies on high- Z , high-density metallic materials, such as iridium and tungsten, have been performed starting from the 1990s, with the aim of developing compact photon converters and high-intensity positron sources [17–20]. Non-scintillating materials were almost exclusively considered, although their light-emitting features allow to directly probe the shower evolution.

Recently, a study on the radiation enhancement by 120-GeV electrons incident on the $\langle 001 \rangle$ axis of a $0.45 X_0$ thick PbWO_4 crystal has been performed [21]. It was the first characterization of a SF-induced ($\chi \sim 3.5 \gg 1$) radiation emission enhancement occurring in an oriented inorganic scintillator. No direct measurement of the energy deposited inside the crystalline sample was made. The only other study to date on PbWO_4 crystals was performed with 26 GeV electrons, i.e., at the SF threshold [22]: as stressed by the authors themselves, albeit promising, the results were of limited usage due the absence of a physical model to compare the data with and the need to deepen the investigation by using different particles and probing higher energies – the $\gtrsim 100$ GeV range, where the SF is fully attained.

In this letter we present an unprecedented direct measurement of the shower development acceleration that occurs in oriented crystals in full SF regime. In particular, we have measured the light yield enhancement in PbWO_4 crystals with a photodetection system based on silicon photomultipliers (SiPMs) [23, 24]. To fully probe the shower development modification, we have explored a wide range of sample thicknesses, using both high-energy electrons and photons. Moreover, we have critically compared our results to a Monte Carlo model, demonstrating an excellent agreement. This study demonstrates that the shower formation, and hence the light yield of oriented scintillating crystals, is significantly enhanced with respect to the unoriented case, which contributes to enrich the general understanding of the working principles of crystal-based detectors and may pave the way to the development of innovative electromagnetic calorimeters and preshower, as discussed in the following.

Four oriented PbWO_4 samples were probed, with thicknesses of 0.45 , 1 , 2 and $4.6 X_0$, thus covering the initial part of the shower, in which the most pronounced enhancement is expected. In fact, it is at the shower beginning that the particles have the highest energy and the lowest angle with respect to the primary trajectory, thus the SF effects are maximally attained. Two of the main axes of PbWO_4 were studied: the 0.45 and $4.6 X_0$ (1 and $2 X_0$) crystals were oriented along the $\langle 100 \rangle$ ($\langle 001 \rangle$) axis.

Our studies were performed on the H2 beamline of the CERN SPS [25], using a 120-GeV/ c electron beam with a $\lesssim 100$ μrad divergence. The $1 X_0$ crystal was also probed with a 5–100 GeV tagged photon beam [26]. The crystals were installed on a high-precision goniometer, which allowed for a fine tuning of the sample-to-beam alignment with 1 μrad precision [27]. The incident particle trajectories were reconstructed with a tracking system based on

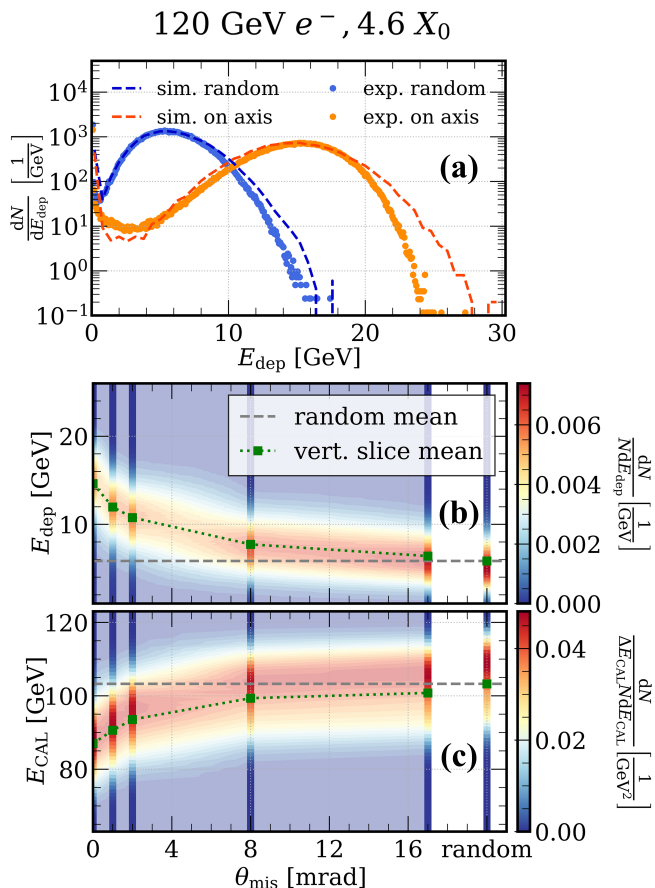


FIG. 2. Measurements by 120 GeV electrons in the $4.6 X_0$ sample. (a) Distribution of E_{dep} in the crystal in randomly oriented and axial configurations, and corresponding simulated (dashed) curves. (b) E_{dep} and (c) E_{CAL} as a function of θ_{mis} . The vivid (shaded) parts of the contour plot correspond to the experimental data (a graphical interpolation). The green squares indicate the mean values at different angles. The abscissa corresponding to the randomly oriented configuration is not to scale.

silicon microstrip detectors, with an overall angular resolution of a few μrad [28]. The energy deposited inside the samples, E_{dep} , was evaluated from the scintillation light measured with the SiPMs. In addition, the energy of all the particles emerging from the crystals, E_{CAL} , was measured by a homogeneous electromagnetic calorimeter consisting of an array of lead glass blocks. The layout of the experimental setup used with electrons is shown in figure 1 bottom. A detailed description can be found, e.g., in [11, 29, 30].

Each crystal sample was probed at different θ_{mis} , from the axial ($\theta_{\text{mis}} = 0 \text{ mrad}$) up to the condition of random orientation ($\theta_{\text{mis}} \sim 50 \text{ mrad} \sim 3^\circ$). The on-axis and random data were compared to the results of Monte Carlo simulations performed using the Geant4 toolkit [31], properly modified to include the SF effects: the custom physics model that we developed is based on the Baier-Katkov quasi-classical operator method [2]. This

method [32–34] is used to rescale the radiation emission and pair production cross sections in oriented crystals inside the Geant4 toolkit [35, 36].

The distribution of E_{dep} in the $4.6 X_0$ crystal – i.e., the thickest sample that was tested, hence the one in which the shower develops the furthest – by 120 GeV electrons, both in random and on-axis alignment, is shown in figure 2a. The calibration of the experimental data into GeV was performed by equalizing the measured random-orientation scintillation peak with the corresponding simulated energy deposit peak. An excellent agreement between the measured E_{dep} spectrum and the simulated energy deposit spectrum has been found in both the alignment conditions. Figure 2b shows the measurements obtained at different θ_{mis} . The energy deposited inside the crystal grows as its alignment approaches the axial configuration: the measured mean E_{dep} is about 5 GeV in random orientation and 15 GeV on axis. The energy deposit enhancement is particularly pronounced up to $\theta_{\text{mis}} = \Theta_0 \sim 0.9 \text{ mrad}$. Furthermore, a lesser enhancement is still attained at 17 mrad (1°). On the contrary, since the downstream calorimeter collects most of the particles emerging from the crystal, E_{CAL} grows with θ_{mis} , as shown in figure 2c. A missing energy ($120 \text{ GeV} - E_{\text{dep}} - E_{\text{CAL}}$) of a few GeV is observed: it is due to transverse losses from particles emerging from the crystal at a large angle, out of the geometric acceptance of the calorimeter, as confirmed by the Monte Carlo.

The $1 X_0$ sample was probed with both electrons and photons. Figure 3 left shows the distribution of the energy deposited in the crystal by the electron beam at different θ_{mis} : as in the previous case, E_{dep} decreases at increasing angle. On the other hand, figure 3 right shows the average energy deposited inside the same crystal sample by the photon beam as a function of the inferred photon energy, $E_\gamma^{\text{inf}} = E_{\text{dep}} + E_{\text{CAL}}$, for different θ_{mis} : on-axis, 0.9 mrad ($1 \Theta_0$), 1.8 mrad ($2 \Theta_0$) and random. The energy deposited on axis grows significantly with E_γ^{inf} up to the maximum available photon energy, i.e., 100 GeV. The extrapolated values at 120 GeV are in good agreement with the ones obtained with 120 GeV electrons, shown in figure 3 left. It is also worth noting that a lesser axis-to-random enhancement was observed even at $E_\gamma^{\text{inf}} \lesssim 25 \text{ GeV}$, i.e., with $\chi < 1$. Overall, all the results are in excellent agreement with the predictions of the simulation model – dashed lines in figure 3 right.

Finally, we exploited the rich set of experimental data we collected with the electron beam to probe the shower development features as a function of the crystal thickness. The mean energy deposited measured in random ($E_{\text{dep}}^{\text{rnd}}$) and axial ($E_{\text{dep}}^{\text{ax}}$) configuration as a function of the sample thickness is shown in figure 4a. Both $E_{\text{dep}}^{\text{rnd}}$ and $E_{\text{dep}}^{\text{ax}}$ increase with the crystal thickness, ranging from a few MeV, in case of sub- X_0 crystals, to the multi-GeV scale in the $4.6 X_0$ sample.

It is particularly interesting to study the difference between $E_{\text{dep}}^{\text{ax}}$ and $E_{\text{dep}}^{\text{rnd}}$, which depends heavily on the crystal thickness, as it is shown in figure 4b. At $1 X_0$, it

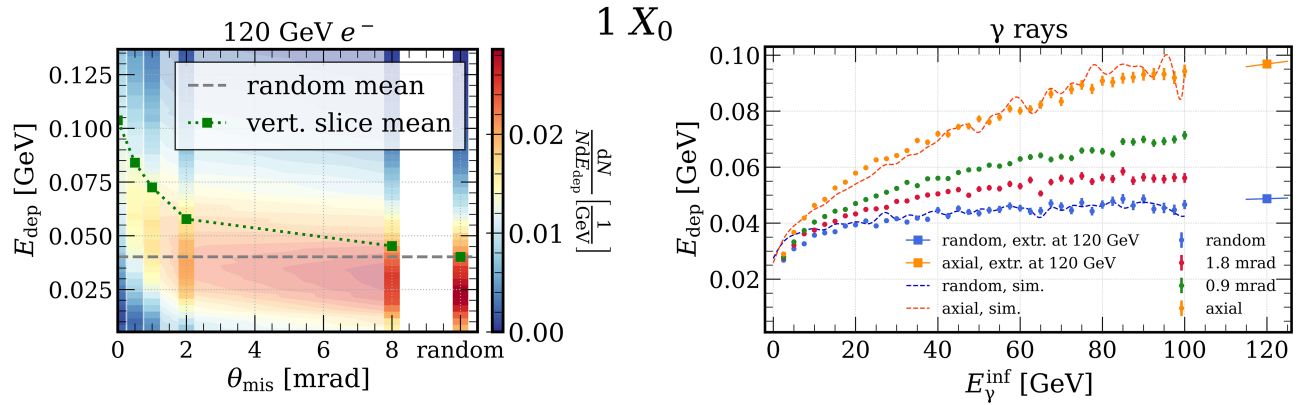


FIG. 3. Measurements on the $1 X_0$ sample. Left: E_{dep} by 120 GeV electrons as a function of θ_{mis} . The vivid (shaded) parts of the contour plot correspond to the experimental data (a graphical interpolation). The green squares indicate the mean values at different angles. The angle corresponding to randomly oriented configuration is not to scale. Right: mean E_{dep} by bremsstrahlung photons as a function of their energy, at different θ_{mis} . The corresponding simulation curves (dashed lines) and extrapolations at 120 GeV (squares) are also shown for the randomly oriented and axial cases. The extrapolations have been computed by fitting the experimental data to a logarithmic function.

corresponds to a very small fraction of the beam energy ($< 0.05\%$). On the other hand, the value grows up to about 8% at $4.6 X_0$. Figure 4c shows the ratio between $E_{\text{dep}}^{\text{ax}}$ and $E_{\text{dep}}^{\text{rnd}}$. This provides an estimate of the energy deposit enhancement measured on axis with respect to the random case, which reaches the maximum value of about 3.8 at $2 X_0$.

The experimental data are compared to the simulated fraction of primary energy deposited per radiation length as a function of the penetration depth inside an ideal, very thick ($> 20 X_0$) crystal. These simulations suggest that the peak in figure 4c should be located around $1.7 X_0$. Above this value, the curve decreases monotonically. The total absorption is reached more gradually than if the development of the entire shower were accelerated by the same amount independently on the penetration depth: as the latter grows, the intensity of the SF effects to the secondary particles decreases (as their average energy does) and their opening angle with respect to the crystal axis can become larger than Θ_0 . As a consequence, at an advanced stage of development the full SF regime is conserved only by a fraction of the particles, and the axis-borne shower proceeds similarly to that occurring in random orientation.

The observed shower acceleration and the corresponding light yield enhancement may truly influence the understanding of homogeneous calorimeters in general, including scenarios in which the particles might be aligned with the lattice axes by chance. In fact, this understanding could help improve the interpretation of data from existing detectors, since commonly used crystals are grown at a small angle with respect to one of the main lattice axes, which is the case of, e.g., the CMS ECAL [37]. The effect of accidentally aligned channels would be particularly significant in case of calorimeters with longitudinal segmentation, such as space-borne γ - and cosmic-

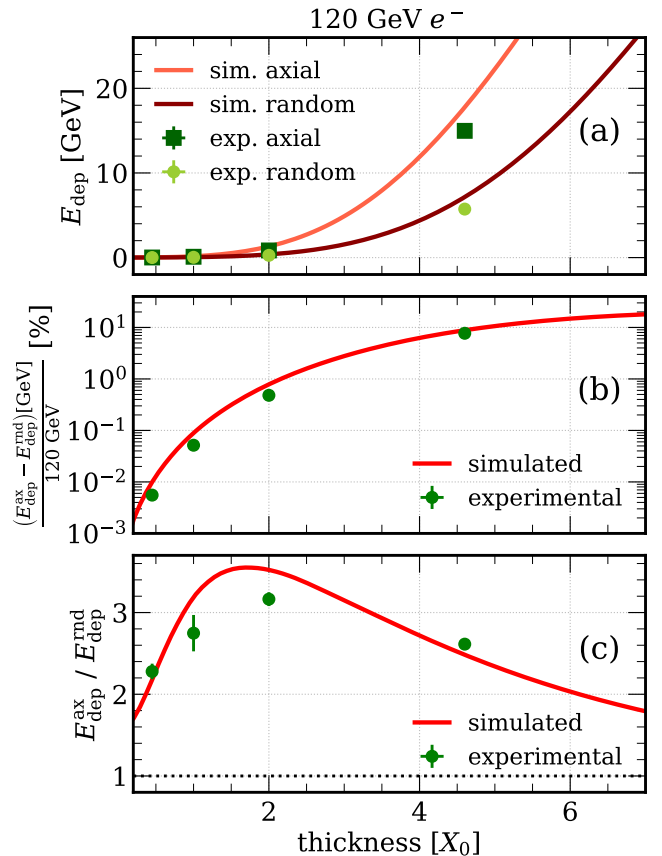


FIG. 4. Measurements performed with the 120 GeV electron beam as a function of the crystal thickness. a: mean E_{dep} in axial and random alignment. b: difference between $E_{\text{dep}}^{\text{rnd}}$ and $E_{\text{dep}}^{\text{ax}}$ normalized to the beam energy. c: ratio between $E_{\text{dep}}^{\text{rnd}}$ and $E_{\text{dep}}^{\text{ax}}$.

ray detectors like the Fermi Large Area Telescope (LAT) [38] and the CALET Total Absorption Calorimeter [39], which feature a segmentation pitch of 1–2 X_0 . It will also be critical to keep the lattice orientation under control in the design of future experiments at the energy frontier, e.g., at the Future Circular Collider [40] and at the Muon Collider [41] – whose crystal calorimeters may have a segmentation pitch of 4–5 X_0 .

Furthermore, our results may prove to be advantageous in the development of next-generation ECALs, operating from the GeV to the multi-TeV scale, that would exploit the SF effects. In practice, in case of forward-geometry experiments, these effects lead to an improvement of the shower containment in the active volume of the detector, which would result in a major improvement of its energy resolution. This is especially true for the first layer of a longitudinally segmented calorimeter with a pitch of a few X_0 , as shown in figure 4c, and is expected to be even more important at higher primary energies, at which the SF effects are stronger and the shower containment enhancement is more pronounced [42]. In addition, this work demonstrates that an ECAL with the same resolution as the current state of the art but with reduced thickness is feasible. This would prove particularly appealing in case of a satellite-borne γ -ray detector with pointing capabilities. Indeed, since one of the main limitations of high-energy photon observation from space is the low photon flux, a thickness reduction would allow for an increase of the calorimeter transverse size and, hence, of its acceptance, while keeping the satellite within the weight and volume constraints of a payload launch. This concept could also be applied to the case of ECALs in fixed-target experiments – such as NA64 at CERN [43], which is currently considering a PWO-based detector – as well as in the forward region of collider experiments.

The improved shower containment also results in an enhancement of high-energy γ -ray detection efficiency. Furthermore, since the hadronic interactions are not affected by the crystalline structure of the bulk, a highly compact oriented crystal calorimeter would be more transparent to the passage of hadrons (see, e.g., [44, 45]) and, if segmented, would have more γ /hadron discrimination power [46]. These features are particularly appealing for accelerator-based forward-geometry experiments that exploit neutral hadron beams as well as for space-borne

γ -ray telescopes.

In summary, our study has provided detailed measurements concerning the electromagnetic shower longitudinal development and the resulting scintillation light yield in axially oriented PbWO_4 crystals with thicknesses between 0.45 and 4.6 X_0 . These experiments, whose results show an excellent agreement with our simulation model, offer a direct insight into the acceleration of shower development in oriented crystals with respect to the randomly oriented case. Notably, this enhancement extends over an angular range of more than 1 mrad, with a detectable effect up to 1° . Since the measurements were performed on samples that are similar in size and growth technique to the ones employed in existing particle detectors, such as electromagnetic calorimeters in HEP and γ -ray astrophysics, these findings highlight the significance of considering the lattice structure of crystalline scintillators, which is currently neglected. Keeping this aspect under control is crucial in order to fully understand the detector performance and can be exploited to substantially enhance the performance of future calorimeters and preshowers at the energy frontier.

ACKNOWLEDGMENTS

This work was primarily funded by INFN CSN5 through the STORM project (P.I. L. Bandiera). We also acknowledge partial support of INFN CSN5 (OREO and Geant4-INFN projects) and CSN1 (NA62 experiment; RD-FLAVOUR project), of the Italian Ministry of University and Research (PRIN 2022Y87K7X) and of the European Commission (Horizon 2020 MSCA-RISE N-LIGHT, GA 872196; Horizon 2020 AIDAInnova, GA 101004761; Horizon 2020 MSCA IF Global TRILLION, GA 101032975; Horizon EIC Pathfinder Open TECHNOCLS, GA 101046458).

We thank CRYTUR, spol. s.r.o. (Turnov, Czech Republic) and Molecular Technology (MolTech) GmbH (Berlin, Germany) for providing the crystals. Moreover, we thank the CERN PS/SPS coordinator and the SPS North Area staff for their support in the setup preparation: in particular, we are indebted to P. Boisseau-Bourgeois, S. Girod, M. Lazzaroni and B. Rae.

-
- [1] C. W. Fabjan and F. Gianotti, Calorimetry for particle physics, *Rev. Mod. Phys.* **75**, 1243 (2003).
 - [2] V. N. Baier, V. M. Katkov, and V. V. Strakhovenko, *Electromagnetic processes at high energies in oriented single crystals* (World Scientific, 1998).
 - [3] U. I. Uggerhøj, The interaction of relativistic particles with strong crystalline fields, *Rev. Mod. Phys.* **77**, 1131 (2005).
 - [4] V. G. Baryshevskii and V. V. Tikhomirov, Synchrotron-type radiation processes in crystals and polarization phenomena accompanying them, *Sov. Phys. Usp.* **32**, 1013 (1989).
 - [5] A. H. Sørensen, Channeling, bremsstrahlung and pair creation in single crystals, *Nucl. Instrum. Methods Phys. Res. B* **119**, 2 (1996).
 - [6] M. Buchanan, Past the Schwinger limit, *Nature Phys.* **2**, 721 (2006).
 - [7] J. C. Kimball and N. Cue, Quantum electrodynamics and channeling in crystals, *Phys. Rep.* **125**, 69 (1985).
 - [8] V. G. Baryshevskii and V. V. Tikhomirov, Creation

- of transversely polarized high-energy electrons and positrons in crystals, *Sov. Phys. JETP* **58**, 135 (1983).
- [9] V. G. Baryshevskii and V. V. Tikhomirov, Pair production in a slowly varying electromagnetic field and the pair production process, *Phys. Lett. A* **113**, 335 (1985).
- [10] Particle Data Group, Review of Particle Physics, *Prog. Theor. Exp. Phys.* **2022**, 083C01 (2022).
- [11] M. Soldani, *Innovative applications of strong crystalline field effects to particle accelerators and detectors*, Ph.D. thesis, Università degli Studi di Ferrara (2023).
- [12] F. J. Dyson and H. Überall, Anisotropy of bremsstrahlung and pair production in single crystals, *Phys. Rev.* **99**, 604 (1955).
- [13] G. Diambrini-Palazzi, Interazioni di fotoni ed elettroni di alta energia in cristalli, *Nuovo Cim.* **25**, 88 (1962).
- [14] J. U. Andersen *et al.*, Channeling radiation, *Annu. Rev. Nucl. Part.* **33**, 453 (1983).
- [15] N. Cue *et al.*, Observation of electric synchrotron radiation in a crystal, *Phys. Rev. Lett.* **53**, 972 (1984).
- [16] A. Belkacem *et al.*, Observation of enhanced pair creation for 50-110-gev photons in an aligned ge crystal, *Phys. Rev. Lett.* **53**, 2371 (1984).
- [17] R. Moore *et al.*, Measurement of pair-production by high energy photons in an aligned tungsten crystal, *Nucl. Instrum. Methods Phys. Res. B* **119**, 149 (1996).
- [18] K. Kirsebom *et al.*, Pair production by 5–150 GeV photons in the strong crystalline fields of germanium, tungsten and iridium, *Nucl. Instrum. Methods Phys. Res. B* **135**, 143 (1998).
- [19] X. Artru *et al.*, Summary of experimental studies, at CERN, on a positron source using crystal effects, *Nucl. Instrum. Methods Phys. Res. B* **240**, 762 (2005).
- [20] L. Bandiera *et al.*, Crystal-based pair production for a lepton collider positron source, *Eur. Phys. J. C* **82**, 699 (2022).
- [21] L. Bandiera *et al.*, Strong reduction of the effective radiation length in an axially oriented scintillator crystal, *Phys. Rev. Lett.* **121**, 021603 (2018).
- [22] V. Baskov *et al.*, Electromagnetic cascades in oriented crystals of garnet and tungstate, *Phys. Lett. B* **456**, 86 (1999).
- [23] M. Soldani *et al.*, A high-performance custom photodetection system to probe the light yield enhancement in oriented crystals, *J. Phys. Conf. Ser.* **2374**, 012112 (2022).
- [24] A. Selmi *et al.*, Experimental layout for the direct measurement of electromagnetic shower acceleration in an oriented crystal scintillator, *Nucl. Instrum. Methods Phys. Res. A* **1048**, 167948 (2023).
- [25] D. Banerjee *et al.*, *The North Experimental Area at the CERN Super Proton Synchrotron*, Tech. Rep. (2021) CERN-ACC-NOTE-2021-0015.
- [26] P. Monti-Guarnieri *et al.*, Beam test characterization of oriented crystals in strong field conditions, *PoS ICHEP2022*, 342 (2022).
- [27] L. Bandiera *et al.*, On the radiation accompanying volume reflection, *Nucl. Instrum. Methods Phys. Res. B* **309**, 135 (2013).
- [28] D. Lietti *et al.*, A microstrip silicon telescope for high performance particle tracking, *Nucl. Instrum. Methods Phys. Res. A* **729**, 527 (2013).
- [29] P. Monti-Guarnieri, Development of an advanced modular setup for the on beam characterization of oriented crystals, *Nuovo Cim. C* **46**, 98 (2023).
- [30] A. Selmi, *Electromagnetic Shower Development in Oriented Crystals*, Master's thesis, Università degli Studi dell'Insubria (2022).
- [31] S. Agostinelli *et al.*, Geant4—a simulation toolkit, *Nucl. Instrum. Methods Phys. Res. A* **506**, 250 (2003).
- [32] V. Guidi, L. Bandiera, and V. Tikhomirov, Radiation generated by single and multiple volume reflection of ultrarelativistic electrons and positrons in bent crystals, *Phys. Rev. A* **86**, 042903 (2012).
- [33] L. Bandiera, E. Bagli, V. Guidi, and V. V. Tikhomirov, Radcharm++: A c++ routine to compute the electromagnetic radiation generated by relativistic charged particles in crystals and complex structures, *Nucl. Instrum. Methods Phys. Res. B* **355**, 44 (2015).
- [34] A. I. Sytov, V. V. Tikhomirov, and L. Bandiera, Simulation code for modeling of coherent effects of radiation generation in oriented crystals, *Phys. Rev. Accel. Beams* **22**, 064601 (2019).
- [35] V. Baryshevsky *et al.*, On the influence of crystal structure on the electromagnetic shower development in the lead tungstate crystals, *Nucl. Instrum. Methods Phys. Res. B* **402**, 35 (2017).
- [36] L. Bandiera, V. Haurylavets, and V. Tikhomirov, Compact electromagnetic calorimeters based on oriented scintillator crystals, *Nucl. Instrum. Methods Phys. Res. A* **936**, 124 (2019).
- [37] P. Lecoq, A. Getkin, and M. Korzhik, *Inorganic Scintillators for Detector Systems* (Springer, 2017) Chapter 8 and references therein.
- [38] W. B. Atwood *et al.*, The large area telescope on the fermi gamma-ray space telescope mission, *Astrophys. J.* **697**, 1071 (2009).
- [39] Y. Asaoka *et al.*, Energy calibration of calet onboard the international space station, *Astropart. Phys.* **91**, 1 (2017).
- [40] M. Lucchini *et al.*, New perspectives on segmented crystal calorimeters for future colliders, *J. Instrum.* **15** (11), P11005 (2019).
- [41] S. Ceravolo *et al.*, Crilin: A crystal calorimeter with longitudinal information for a future muon collider, *J. Instrum.* **17** (09), P09033 (2017).
- [42] L. Bandiera *et al.*, A highly-compact and ultrafast homogeneous electromagnetic calorimeter based on oriented lead tungstate crystals, *Front. Phys.* **11**, 10.3389/fphy.2023.1254020 (2023).
- [43] D. Banerjee, NA64—Search for Dark Sector Particles, in *Advances in Cosmology*, edited by M. Streit-Bianchi, P. Catapano, C. Galbiati, and E. Magnani (2022) pp. 183–193.
- [44] E. Cortina Gil *et al.*, *HIKE, High Intensity Kaon Experiments at the CERN SPS: Letter of Intent*, Tech. Rep. (2022) CERN-SPSC-2022-031, SPSC-I-257, SPSC-I-257.
- [45] HIKE Collaboration, *High Intensity Kaon Experiments (HIKE) at the CERN SPS: Proposal for Phases 1 and 2*, Tech. Rep. CERN-SPSC-2023-031, SPSC-P-368 (2023).
- [46] P. Monti-Guarnieri, Particle identification with a longitudinally segmented homogeneous calorimeter composed of oriented crystals, (2024), In preparation.